ISSN 1027-4510, Journal of Surface Investigation. X-ray, Synchrotron and Neutron Techniques, 2011, Vol. 5, No. 1, pp. 1–6. © Pleiades Publishing, Ltd., 2011.
Original Russian Text © V.G. Kohn, T.C. Argunova, Jung Ho Je, 2011, published in Poverkhnost'. Rentgenovskie, Sinkhrotronnye i Neitronnye Issledovaniya, No. 1, pp. 5–10.

Features in Phase-Contrast Images of Micropipes in SiC in White Synchrotron Radiation Beam

V. G. Kohn[a], T. C. Argunova[b], and Jung Ho Je[c]

[a] *Kurchatov Institute of Atomic Energy, ul. Kurchatova 46, Moscow, 123182 Russia*
e-mail: kohnvict@yandex.ru

[b] *Ioffe Physical Technical Institute, Russian Academy of Sciences, ul. Politekhnicheskaya 26, St. Petersburg, 194021 Russia*
e-mail: argunova2002@mail.ru

[c] *Pohang University of Science and Technology, San 31, Hyoja-dong, Nam-gu Pohang, South Korea 790-784*

Received March 22, 2010

Abstract—An interesting feature in phase-contrast images of micropipes in silicon carbide in white synchrotron radiation beam was experimentally studied and theoretically explained. This feature consists in that a change in micropipe cross-section sizes does not lead to changes in its image sizes, but has an effect only on the contrast. The experiment was performed on the synchrotron radiation source in Pohang, South Korea. On the one hand, this effect is explained by a small phase progression caused by the micropipe, and, on the other hand, by satisfying the conditions for Fraunhofer diffraction, when the transverse micropipe size is smaller than the first Fresnel zone diameter. As a rule, the near-field conditions are satisfied in X-ray optics when only object edges are imaged. However, micropipes are so small that the standard edge theory is inapplicable. A universal intensity distribution profile was obtained for micropipes with very small cross sections.

DOI: 10.1134/S1027451011010125

INTRODUCTION

Silicon carbide crystals grown by sublimation contain crystal structure defects such as stacking faults, dislocations, dislocation micropipes, and microvoids. There is the correlation between poor characteristics of SiC-based devices and their structure defectness [1]. Micropipes and microvoids formed in the crystal volume during growth are especially dangerous, since they cause degradation of devices and can completely disable them. Progress in SiC crystal growth technologies led to the appearance of samples with very low micropipe concentrations, i.e., ~0.7 cm^{-2} [2]. However, production of SiC-based devices of power semiconductor electronics requires a further decrease in the density of these defects [3]. Therefore, it is important to detect micropipes during crystal production to adequately estimate the yield of high-quality devices.

Defect transformation during crystal growth is characteristic of silicon carbide. Defects of different types can interact, merge, dissociate, be annihilated, and change their nature. Micropipes dissociate with the formation of screw dislocations [4, 5]. They react with each other [6, 7] and boundaries of inclusions of other polytypes [7–9]. The interaction of micropipes is accompanied by changing their cross-section sizes [6, 7, 10]. The micropipe morphology is controlled by both the type of dislocations connected with them [11] and the conditions of their nucleation and interaction [6–9]. The interaction of defects causes a change in their density distribution, which decreases due to annihilation, dissociation, and merging processes. Since the cross-section size and morphology of the micropipe depend on its reactions with other defects, the knowledge of these parameters aids in anticipating and controlling the micropipe density.

The micropipe distribution is observed using an optical microscope on etch pits on the SiC wafer surface. The etch pit size is not equal to the micropipe cross-section size, and the hexagonal pit shape does not reflect its morphology. One of the direct methods for studying the micropipe size and morphology is X-ray topography in combination with numerical simulation of images [12, 13]. However, elastic fields of dislocation micropipes are exposed to fields of other defects, i.e., neighboring micropipes, dislocations, and low-angle boundaries. When defect strain fields overlap in topographic images, micropipe characteristic determination becomes impossible.

Recently, an alternative direct method for observing micropipes, i.e., phase contrast in the synchrotron radiation (SR) beam [6–10], was successfully developed. Third-generation SR sources have a small angular size and provide high spatial coherence of radiation. At the same time, even the initial SR spectrum, i.e., without monochromatization, is shaped as a curve with a maximum at a certain energy in the case at hand. A decrease in the radiation intensity at high and low energies is caused by the SR generation's nature and absorption in the sample, respectively. Therefore, even "white" SR is in part coherent, which is quite

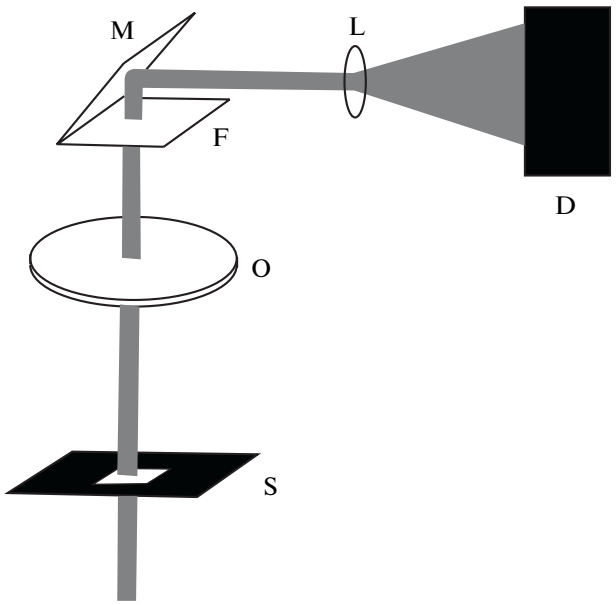

Fig. 1. Experimental scheme: the synchrotron radiation beam is upward; S is the entrance slit; O is the sample (silicon carbide crystal containing micropipes); F is the scintillator crystal 200 μm thick, absorbing X-ray photons and emitting optical photons; M is the mirror; L is the lens system magnifying the image; and D is the coordinate detector (CCD array).

sufficient for recording phase-contrast images of small objects such as micropipes in SiC.

The technique for measuring in white SR has a number of advantages over the use of a monochromator, i.e., high intensity, short exposure time, large exposed area, and simple experimental equipment. The simple scheme, high intensity, and wide wavelength range make it possible to combine various research methods during a single experiment, combining phase-contrast imaging with alternative methods, including analytical techniques. A significant disadvantage of the modern approach is that obtained information is mostly qualitative. Successful visualization of the microstructure provokes measurements of various characteristics, including sizes of its elements, directly on images.

However, the phase contrast nature is such that image sizes are not equal to sizes of imaged objects themselves.

The problem of obtaining reliable information can be solved by developing the methods of numerical simulation of phase-contrast images of objects of various shape and size. Such an approach was recently proposed [14] based on Kirchhoff integral calculation for monochromatic SR harmonics followed by summation over an actual spectrum, taking into account absorption in the sample. Slightly later, the FIMTIM program was developed for automatic determination of the parameters of the elliptic micropipe cross section using the beam from the good-fit condition for calculated and experimental profiles of relative intensity. It was shown that the tube cross section can vary not only its size, but also orientation, during its growth [15, 16]. However, image variations depending on micropipe sizes and cross-section shape have not been systematically studied.

In this study, we consider an interesting feature of phase-contrast images of micropipes, i.e., that the image size is almost independent of the elliptic cross-section diameter for characteristic sample–detector distances from 10 to 50 cm.

As cross-section diameters decrease, only the contrast decreases. An appreciable change in the contrast in experimental images of the micropipe as it moves along its axis was a mysterious and puzzling phenomena, since it seemed that there was no cause of such a decrease. This mystery is explained in this paper.

It turns out that the change in the contrast is an indication of a change in the cross section of the tube itself, rather than a change in any condition external to the tube.

EXPERIMENTAL

The 4H-SiC crystal studied in this work was grown by sublimation [17] in argon atmosphere at a temperature of 2200°C with a rate of 300 μm/h. The growth axis was parallel to the [0001] direction. The crystal was cut into wafers parallel to the growth axis. Micropipes with axes as a rule parallel to the growth axis were arranged almost parallel to the sample surface.

Phase-contrast images were obtained at the 7B2 station (X-ray microscopy) of the third-generation SR source in Pohang (Pohang Light Source). A bending magnet provided effective source sizes of 60 and 160 μm in vertical and horizontal directions, respectively. The source was at a distance of 34 m from the sample. The effective emission spectrum was calculated using the initial source spectrum in the energy range from 5 to 40 keV, which is shaped as a monotonically decreasing curve. Taking into account absorption in a beryllium window 2 mm thick and in the SiC wafer 450 μm thick, the spectrum gained a pronounced maximum at an energy of 16 keV [14–16].

Samples were fixed on a holder providing movement along three axes with an accuracy of 0.1 μm, turns, and rotation about the vertical axis. The sample surface was aligned perpendicular to the beam; the micropipe axes were positioned horizontally in order to use the minimum angular size of the source in the vertical direction. Radiation passing through the sample arrived at a $CdWO_4$ scintillator crystal 200 μm thick and excited its luminescence. Visible light was reflected from the specularly polished silicon wafer and was directed to a detector with a CCD array. The experimental scheme is shown in Fig. 1. We can see that the light image is magnified by a lens system and then is recorded by the detector. The image magnifica-

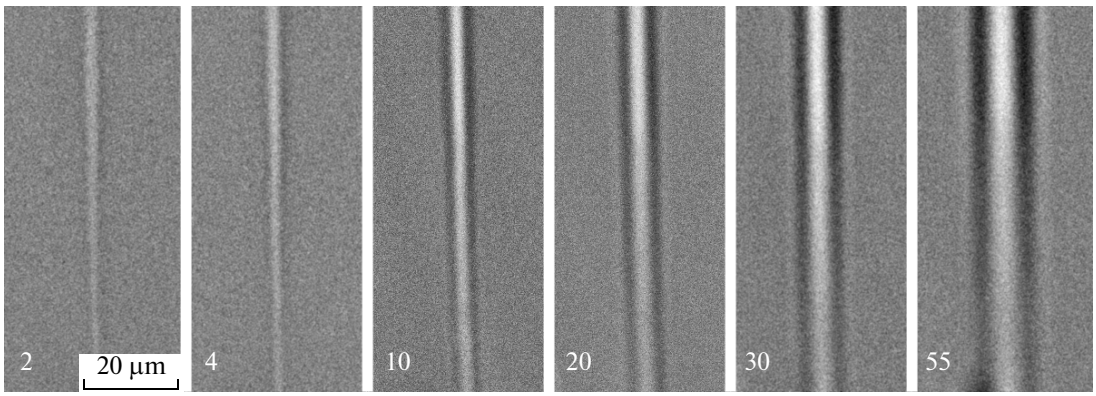

Fig. 2. Series of images of an isolated micropipe, obtained at various distances given in centimeters by numerals in fragments.

tion can be varied from 1 to 50 times. The detector recorded images in the numerical form with a resolution of 14 bits per an array 1600 × 1200 pixels in size. The field of view was 310 μm (H), which corresponds to a pixel size of 0.194 μm.

As shown previously, the image sizes and structure depend on the sample–detector distance [14–16]; therefore, this distance was varied during measurements. The experimental scheme allowed variation of this distance from 5 mm to 1.5 m. In fact, a series of micropipe images at distances from 5 to 50 cm was measured.

Micropipes with a cross section of the order of several micrometers and smaller are phase objects the contrast of which depends strongly on the tube axis orientation with respect to the SR beam axis. The central area of images can be both white and black; moreover, various areas of the same tube can have different contrasts. The numerical simulation method was based on the assumption that the tube is homogeneous along its axis; hence, it is sufficient to calculate the intensity distribution in the direction perpendicular to the beam and tube axis. This assumption is quite valid at a tube orientation such that its axis is almost perpendicular to the beam. Therefore, we studied orientations of micropipes when their axes were almost perpendicular to the beam and were arranged horizontally, so that the contrast was formed by the vertical (smallest) focus size.

Figure 2 shows a series of images of a region of one micropipe obtained at various distances from the sample. Numerals in images indicate the distance in centimeters. This series was specially selected to show the feature detected in the micropipe image. In two left images obtained at distances of 2 and 4 cm, the horizontal size (cross-section diameter) monotonically decreases when moving downward along the tube axis. Assuming that the size of the image obtained at a distance of 2 cm correlates with the actual size of the micropipe cross section, we can conclude that the micropipe cross section decreases when moving downward. However, the image contrast is very small at short distances and special conditions are required to detect it. Therefore, images are often obtained at distances from 10 to 50 cm. However, the image structure changes significantly at these distances. Black bands appear along the bright band edges; at longer distances, additional bright bands are observed. It is interesting that the distance between black bands already does not change when moving downward in these images, i.e., the intensity distribution profile in the horizontal direction is the same at all heights. Only the image contrast changes.

Another important feature is the fact that the distance between black bands increases with the sample–detector distance z. This image can be scaled, and it is easy to estimate that the scale factor is proportional to $z^{1/2}$ From this circumstance, two conclusions follow: the micropipe image structure at long distances is universal independently of its cross sections, and actual micropipe sizes at these distances appear only through the contrast.

Figure 3 shows the image of another micropipe. For this micropipe, the experimental profiles of the relative intensity distribution in the vertical direction in various regions along the tube axis were obtained. Cross-section diameters were quantitatively determined by comparing the results of numerical simulation of the intensity profile for various cross-section diameters with the experimental profile. The FIMTIM program was used. The calculation results are shown in the figure. We can see that the transverse tube diameter halved in the region of decreasing contrast. The longitudinal diameter also slightly decreased, although it was very small as before.

THEORY

As noted in [14–16], phase-contrast images of micropipes in the white SR beam are in fact formed as an incoherent superposition of images for various harmonics; in this case, the weight of each harmonic (effective emission spectrum) should be calculated taking into account its absorption on the path from the

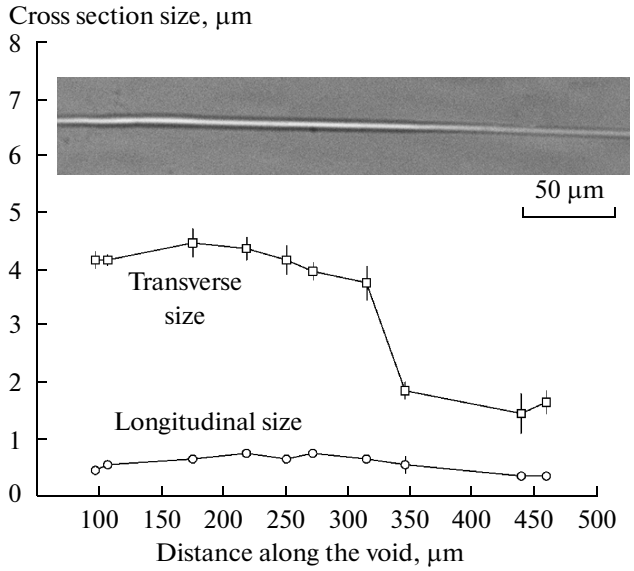

Fig. 3. Image of an isolated micropipe (upper fragment) and the dependence of transverse and longitudinal diameters of its cross section on the position along the micropipe axis. The diameters were obtained by fitting using the FIMTIM program of numerical simulation of images. We can see that the transverse diameter changes almost twice, while the image size was almost unchanged.

source to the detector. The consideration of absorption in the sample leads to a radical change in the effective spectrum. It has a maximum at photon energy $E = 16$ keV and sharply decreases with decreasing energy. That is, even in the absence of a monochromator, the actual spectrum forming the image is localized near 16 keV. We note that it is impossible to change—moreover, to vary—the energy in experiments with the white SR beam.

To calculate the monochromatic image, the micropipe can be represented as a quasi-linear object that rapidly or slowly changes the phase of the wave passing through it when moving across or along the axis, respectively. By separating the relative intensity profile in any cross section across the axis, we can neglect the dependence along the axis. In this approximation, the intensity profile can be described using the single integral in infinite limits,

$$I(x) = |a(x_0)|^2,$$
$$a(x_0) = \int dx_1 P_K(x_0 - x_1, Z) T(x_1), \quad x_0 = x\frac{z_0}{z_t}. \tag{1}$$

Here z_0 is the source–object distance, z_1 is the object–detector distance, $z_t = z_0 + z_1$, and $Z = z_0 z_1 / z_t$. Thus, the problem is reduced to calculating the convolution of two functions, the first of which is the Kirchhoff propagator

$$P_K(x,z) = \frac{1}{(i\lambda z)^{1/2}} \exp\left(i\pi\frac{x^2}{\lambda z}\right), \tag{2}$$

where λ is the emission wavelength. The second function $T(x)$ describes the effect of the object on the coherent wave. For small-sized objects, it is sufficient to consider changes in the wave phase and amplitude within geometrical optics without changing the beam trajectories, i.e., assuming that all beams are parallel to the optical axis. In this approximation, for a void with an elliptical cross section in a material, we can exclude the homogeneous sample region and consider only wave distortion due to inhomogeneity. Then $T(x) = 1$ at $|x| > R$ and, at $|x| < R$, we have

$$T(x) = \exp\left[(iP + M)\left(1 - \frac{x^2}{R^2}\right)^{1/2}\right],$$
$$P = \frac{2\pi}{\lambda}\delta R_0, \quad M = P\frac{\beta}{\delta}. \tag{3}$$

Here R and R_0 are the radii of the micropipe elliptical cross section across and along the beam, respectively; the complex refractive index of a medium is $n = 1 - \delta + i\beta$. Doubled values of R and R_0, i.e., diameters of the elliptical cross section, are a priori unknown and are to be determined.

Since the integrand in (1) does not decay at infinity, for numerical calculations, it is convenient to rewrite the integral, using the propagator normalization property, in the form

$$a(x_0) = 1 + \int dx_1 P_K(x_0 - x_1, Z)[T(x_1) - 1]. \tag{4}$$

The monochromatic intensity profiles were calculated on a point grid in the range from 5 to 40 keV and then were summed taking into account the spectrum shown in [14–16]. The images were numerically simulated using the FIMTIM program (see [15, 16] for more details).

A large series of calculations was performed, which confirmed the image feature indicated in the previous section, i.e., their universality for typical micropipe cross section diameters no more than 2 μm at relatively long distances, more than 10 cm. It turned out that such universality is a typical manifestation of Fraunhofer diffraction (far-field image) in phase objects under the additional condition that the phase shift P is less than unity.

To better understand physics of such imaging, let us make obvious approximations and simplify the problem. In particular, we can neglect absorption, $M = 0$, and since $z_0 \gg z_1$, we can neglect the distance z_0 finiteness and replace x_0 by x and Z by z_1. We note that the condition $P < 1/2$ for SiC and $E = 16$ keV is satisfied at $R_0 < 1.2$ μm; however, it is exactly the most typical longitudinal micropipe radius. For reference, $\lambda = 0.0775$ nm and $\delta = 2.6 \times 10^{-6}$. Thus, when this condition is satisfied, we can expand the exponent $T(x)$ in a power series and restrict the analysis to only the first term.

We note that the Kirchhoff propagator weakly varies at transverse distances smaller than the radius of the

first Fresnel zone, $r_1 = (\lambda z_1)^{1/2}$. For the above conditions, at a distance of 30 cm, we have $r_1 = 4.8$ μm. However, the transverse radius of almost all micropipes is smaller than this value. This means that the term $\pi (x_1/r_1)^2$ in the propagator phase can be neglected in calculating the integral, which is exactly the typical approximation in the case of Fraunhofer diffraction. Taking into account these approximations, for function (4) we obtain the expression

$$a(x) = 1 + i^{1/2}\frac{2\pi^2\delta}{\lambda r_1}RR_0\exp\left(i\pi\frac{x^2}{r_1^2}\right)b(x), \qquad (5)$$

where

$$b(x) = \frac{2}{\pi}\int_{-1}^{1}dt\exp\left(-2i\pi\frac{xR}{r_1^2}t\right)\left(1-t^2\right)^{1/2} = \frac{2x_0}{x}J_1\left(\frac{x}{x_0}\right), \qquad (6)$$

$$x_0 = \frac{r_1^2}{2\pi R}.$$

Here $J_1(z)$ is the first-order Bessel function. We note that $b(0) = 1$.

The relative radiation intensity is a squared magnitude of (5). Remaining within the approximation linear in R_0, we obtain

$$I(x) = |a(x)|^2 \approx 1 + \frac{4\pi^2\delta}{\lambda r_1}RR_0b(x)\cos\left(\pi\frac{x^2}{r_1^2} + \frac{\pi}{4}\right). \qquad (7)$$

In our opinion, the formula derived allows interesting conclusions. In the central image region, where $|x| < x_0$, the function $b(x)$ is almost equal to unity. Therefore, the intensity variation is independent of micropipe cross section radii and is universal. The universal image is shaped as a Fresnel zone plate with a bright central zone and zone radii $x_n = (4n - 3)(\lambda z_1)^{1/2}/2$. As the distance from the center increases, the oscillation amplitude decreases and vanishes at $|x| = 3.8\,x_0$. Then oscillations appear again and continue to pulse in amplitude. The degree of oscillation damping depends on the transverse radius of the cross section. And the complete contrast is scaled by the product of both radii, i.e., the cross-section area.

In the experiments with the white SR beam, formula (7) should be averaged over the effective emission spectrum. The contrast at the central point varies very weakly in comparison with $E = 16$ keV, as well as the Fresnel zone boundaries. However, the amplitude of lateral oscillations very strongly decreases. Therefore, even a weak dependence of the contrast on the transverse radius disappears and the intensity profile becomes completely universal. The only information on the micropipe structure that can be obtained by the contrast at the central image point is its cross-section area. Figure 4 shows the universal curve $C(u) = (\langle I(x)\rangle - 1)\,R_1^2/(RR_0)$, where $u = x/r_1$, $R_1^2 = \lambda r_1/(2^{3/2}\pi^2\delta)$, and the parameters r_1, λ, and δ are calculated for $E = 16$ keV, which corresponds to the emission spectrum maximum, $\langle I(x)\rangle$ is the intensity averaged over the effective emission spectrum. This function is independent of the distance z_1 and micropipe cross-section sizes. Hence, the experimentally measured profile of the micropipe image intensity is described by the formula $\langle I(x)\rangle = 1 + (RR_0/R_1^2)C(x/r_1)$, provided that the above conditions are satisfied.

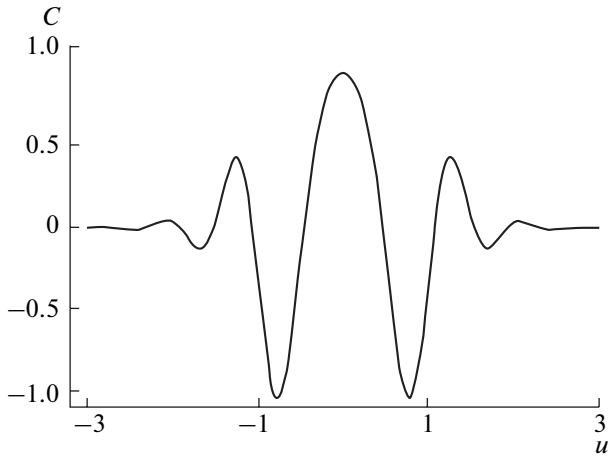

Fig. 4. Universal intensity profile across the image of a small micropipe (see text for details).

CONCLUSIONS

It was shown that the phase contrast method in the white synchrotron radiation beam has limitations when using it for imaging SiC micropipes with relatively small cross sections at long distances. In this case, the wave phase shift caused by the micropipe is less than unity and the perturbation theory is valid, according to which the contrast is simply proportional to the longitudinal radius. At the same time, Fraunhofer diffraction conditions are satisfied in this case. In this diffraction mode, the image is the standard view of Fresnel zones the sizes of which depend only on the sample–detector distance and the micropipe transverse radius simply linearly scales with the contrast. As a result, the image view is standard and the contrast allows determination of only the micropipe cross-section area.

Therefore, to determine the micropipe morphology, it is reasonable to obtain images at sample–detector distances as short as possible and to obtain images at different angles between the micropipe axis and incident beam to increase the longitudinal diameter of the cross section. The developed theory made it possible to explain the features of actually observed images of micropipes in SiC.

REFERENCES

1. Y. Wang, G. Ali, M. Mikhov, et al., J. Appl. Phys. **97**, 013540 (2005).

2. St. G. Müller, M. Brady, A. Burk, et al., Superlattices Microstruct. **40**, 195 (2006).
3. T. Hatakeyama, K. Ichinoseki, K. Fukuda, et al., J. Cryst. Growth **310**, 988 (2008).
4. B. M. Epelbaum and D. Hofmann, J. Cryst. Growth **225**, 1 (2001).
5. R. Yakimova, N. Vouroutzis, M. Syväjärvi, et al., J. Appl. Phys. **98**, 034905 (2005).
6. M. Yu. Gutkin, A. G. Sheinerman, T. S. Argunova, et al., J. Appl. Phys. **94**, 7076 (2003).
7. M. Yu. Gutkin, A. G. Sheinerman, and T. S. Argunova, Phys. Status Solidi C **6**, 1942 (2009).
8. M. Yu. Gutkin, A. G. Sheinerman, T. S. Argunova, et al., J. Appl. Phys. **100**, 093518 (2006).
9. M. Yu. Gutkin, A. G. Sheinerman, T. S. Argunova, et al., Phys. Rev. B **76**, 064117 (2007).
10. M. Yu. Gutkin, A. G. Sheinerman, M. A. Smirnov, et al., Appl. Phys. Lett. **93**, 151905 (2008).
11. J. P. Hirth, Acta Mater. **47**, 1 (1999).
12. X. R. Huang, M. Dudley, W. M. Vetter, et al., Appl. Phys. Lett. **74**, 353 (1999).
13. Yi. Chen, M. Dudley, E. Sanchez, and M. Macmillan, J. Electron. Mater. **37**, 713 (2008).
14. V. G. Kohn, T. S. Argunova, and J.-H. Je, Appl. Phys. Lett. **91**, 171901 (2007).
15. T. S. Argunova, V. G. Kohn, and J.-H. Je, Poverkhnost', No. 12, 48 (2008) [J. Surf. Invest. **2**, 861 (2008)].
16. T. Argunova, V. Kohn, J.-W. Jung, and J.-H. Je, Phys. Status Solidi A **206**, 1833 (2009).
17. Yu. A. Vodakov, A. D. Roenkov, and M. G. Ramm, Phys. Status Solidi B **202**, 177 (1997).

SPELL: 1. ok